



HAL
open science

Engineering of Voltage Controlled Magnetic Anisotropy Magnetic Tunnel Junctions at Cryogenic Temperatures

Pedro Brandao Veiga, Ricardo Sousa, Liliana Buda-Prejbeanu, Stephane Auffret, Isabelle Joumard, Laurent Vila, Ioan-Lucian Prejbeanu, Bernard Diény

► **To cite this version:**

Pedro Brandao Veiga, Ricardo Sousa, Liliana Buda-Prejbeanu, Stephane Auffret, Isabelle Joumard, et al.. Engineering of Voltage Controlled Magnetic Anisotropy Magnetic Tunnel Junctions at Cryogenic Temperatures. IEEE Transactions on Magnetics, 2023, 59 (11), pp.1-5. 10.1109/TMAG.2023.3284503 . hal-04205048

HAL Id: hal-04205048

<https://hal.science/hal-04205048>

Submitted on 12 Sep 2023

HAL is a multi-disciplinary open access archive for the deposit and dissemination of scientific research documents, whether they are published or not. The documents may come from teaching and research institutions in France or abroad, or from public or private research centers.

L'archive ouverte pluridisciplinaire **HAL**, est destinée au dépôt et à la diffusion de documents scientifiques de niveau recherche, publiés ou non, émanant des établissements d'enseignement et de recherche français ou étrangers, des laboratoires publics ou privés.

Engineering of Voltage Controlled Magnetic Anisotropy Magnetic Tunnel Junctions at Cryogenic Temperatures

Pedro Brandao Veiga¹, Ricardo C. Sousa¹, Liliana D. Buda-Prejbeanu¹, Stephane Auffret¹, Isabelle Joumard¹, Laurent Vila¹, Ioan-Lucian Prejbeanu¹ and Bernard Dieny¹
¹SPINTEC, Grenoble Alpes Univ., CEA, CNRS Grenoble, 38000, France

We identified through numerical simulations the optimal condition to have a deterministic switching regime assisted by Voltage Controlled Magnetic Anisotropy (VCMA). To minimize the write energy required to reach this regime, we measure the VCMA coefficient ξ on perpendicular magnetic tunnel junctions (pMTJ) with high resistance-area product (RA) and varying thicknesses of the FeCoB storage layer and the naturally oxidized tunnel barrier. The VCMA coefficient is higher as the effective anisotropy decreases, which is the case for larger Mg and FeCoB thicknesses. The temperature dependence of ξ was shown to increase from room temperature to 5K, showing values up to 35 fJ/Vm at 10K.

Index Terms—Cryoelectronics, MRAM, Spintronics, VCMA.

I. INTRODUCTION

WITH INCREASING DEMANDS for larger computational power outweighing advances in CMOS efficiency, the trend in global energy demand will rapidly increase in the forthcoming years [1]. Cryo-electronics has the potential to overcome the obstacles conventional electronics faces as cooling infrastructures are improved and device efficiency at low temperature could offset the power required for cooling. In particular, magnetic random-access-memories (MRAM) show promising characteristics at low temperature, notably longer retention times, higher tunneling magneto-resistance (TMR) and improved endurance. Among possible writing mechanisms such as spin-transfer-torque (STT), spin-orbit-torque (SOT) and voltage-controlled-magnetic-anisotropy (VCMA), the latter is an inherently promising approach to minimize the write energy per bit (E_{bit}) as it does not rely on current induced switching, greatly reducing Joule dissipation losses. Viability of this technology would require a novel approach in material development, focusing on finding a balance between Ebit and retention time. The simplest structure for a VCMA-MRAM consists of a hard/reference layer (HL), an oxide tunnel barrier (MgO) and a storage/free layer (SL), with reference and storage layers magnetizations collinear in either parallel (P) or anti-parallel (AP) states. The memory retention is determined by the thermal stability factor Δ , defined as $\Delta = (E_B V_{ol}) / (k_B T)$, where E_B is the energy barrier from P to AP state, V_{ol} is the storage layer volume, k_B is the Boltzmann constant and T the temperature at which the memory operate in standby. For a memory working at cryogenic temperatures (for instance at 3K), the same Δ can be maintained reducing E_B by a factor of 100 without losing stability. The critical switching voltage V_C is reduce correspondingly as it is proportional to E_B . The total write energy will consist of the dissipative E_D losses, which can be derived by Ohm's Law $V = RI$ and $E = \int P dt$, where P is power:

$$E_D = \int_0^\tau \frac{V_C^2}{R_P} dt \quad (1)$$

and the capacitive E_C losses, derived by the integration of the work done to charge a capacitor:

$$E_C = \frac{CV_C^2}{2} \quad (2)$$

Where C is the capacitance of the tunnel junction, R_P is the resistance and τ is the writing pulse length. In previous systems using VCMA switching [2] [3] [4], E_D is minimized due to the high parallel resistance state R_P , but it can still be three orders of magnitude larger than E_C [5], limiting how much further improvement can be achieved in such devices. Considering that we can have a factor of 10 reduction of V_C by optimizing E_B , we could achieve $E_{bit}(300K)=100E_{bit}(3K)$, reducing E_D down to 70aJ according to recent work on low energy switching [6].

The voltage controlled magnetic anisotropy, as the name implies, is a modulation of the anisotropy with an applied voltage bias V_b across the tunnel barrier. It has been determined to have a linear effect on the surface anisotropy of the form $K_S(V) = K_{S_0} + \xi V_b / t_{MgO}$ [7] [8], although other results on its nature also suggest a second order dependence [9]. In this expression, ξ is the VCMA coefficient, t_{MgO} is the tunnel barrier thickness and K_{S_0} is the surface anisotropy at zero bias.

II. SIMULATION RESULTS

To investigate the behavior of VCMA at low temperatures, switching probability phase diagrams were calculated using a macrospin model based on the Landau-Lifshitz-Gilbert equation, which governs the magnetization dynamics of a ferromagnet in the presence of a magnetic field, given by:

$$\frac{\partial \vec{m}}{\partial t} = -\gamma(\vec{m} \times \mu_0 \vec{H}_{eff}) + \alpha \left(\vec{m} \times \frac{\partial \vec{m}}{\partial t} \right) + \left(\frac{\partial \vec{m}}{\partial t} \right)_{STT} \quad (3)$$

Where \vec{m} is the magnetization of the layer, γ is the reduced gyromagnetic ratio, μ_0 is the vacuum permeability, \vec{H}_{eff} is the effective field, α is the Gilbert damping and the last term

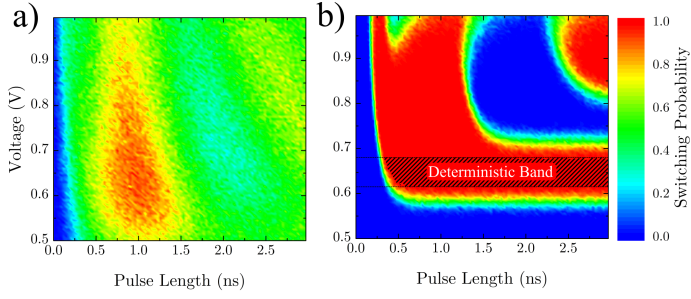


Fig. 1. Simulated switching probability from AP to P state for a) stochastic precessional regime at 300K and b) deterministic regime at 4K highlighted by dashed lines. Parameters of the simulation: 30nm storage layer with retention of $\Delta = 700$ at 10K and VCMA coefficient $\xi = 100 \text{ fJ/Vm}$.

of the equation is the Slonczewski term for spin-transfer (or current-driven) torque [10].

In the context of low energy applications, the chosen parameters for a weak effective anisotropy K_{eff} are: a first order anisotropy $K_1 = 1.06 \text{ mJ/m}^2$, a saturation magnetization $M_S = 0.94 \text{ MA/m}$ and a second order anisotropy $K_2 = -0.175 \text{ mJ/m}^2$, providing an easy cone anisotropy to a storage layer with 30nm in diameter and 2nm thickness [11]. In this VCMA system, we implement the voltage dependent $K_1(V)$ with $\xi = 100 \text{ fJ/Vm}$ and a tunnel barrier of 2nm with a high Gilbert damping of 0.1. Furthermore, a constant in-plane magnetic field $H_{IP} = 9 \text{ mT}$ is used and a voltage pulse of varying length and amplitude was applied for 10^4 attempts, at 4K and 300K.

The precessional dynamics of VCMA results in probability fringes visible at 300K in Fig.1a. At 4K however, a 100% switching region in Fig.1b appears associated to a deterministic switching band between 0.6V and 0.7V. This band defines a critical switching voltage V_C and can be modulated by changing the energy barrier of the system, notably the interfacial anisotropy and magnetization saturation. Taking into account a second order anisotropy K_2 and an in-plane field H_{IP} , we can calculate V_C analytically using the total energy density of the system from Eq.4 [11].

$$\begin{aligned} \varepsilon_T = & -K_1(V)m_z^2 - K_2m_z^4 \\ & - \frac{1}{2}\mu_0M_S^2(N_zm_z - N_xm_x) - \mu_0M_SH_{IP}m_x \end{aligned} \quad (4)$$

Where the first two terms correspond to the perpendicular magnetic anisotropy energy, the third is the expanded demagnetization energy for a finite circular geometry [12] and the fourth is the Zeeman energy. With N_z and N_x the demagnetization tensor diagonal components and m_z and m_x the unitary magnetizations. By taking $\partial\varepsilon_T/\partial\theta = 0$ we can calculate the equilibrium angle θ_{eq} . Having the total energy equals to the energy barrier as $\varepsilon_T(V_b, \theta_{eq}) = -\mu_0M_SH_{IP}$ we arrive at Eq.6.

$$\sin\theta_{eq} = \frac{2 * 3^{\frac{1}{3}}a + 2^{\frac{1}{3}}(-9b + \sqrt{-12a^3 + 81b^2})^{\frac{2}{3}}}{6^{\frac{2}{3}}(-9b + \sqrt{-12a^2 + 81b^2})^{\frac{1}{3}}} \quad (5)$$

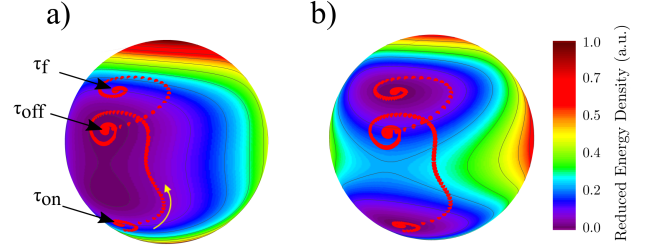


Fig. 2. Representation of the energy density of the system for different applied voltages and the magnetization trajectory during switching in red for a pulse of 1ns. a) 3D Energy landscape at 0.5V (higher than V_C), with τ_{on} , τ_{off} and τ_f being the time of pulse initialization, when the pulse is turned off and the end of the simulation, respectively. The yellow arrow shows the direction of movement of \vec{m} b) 3D Energy landscape at 0V.

$$V_C = \frac{2t_{FeCoB}t_{MgO}}{\xi} \left[\frac{\mu_0M_SH_{IP}(1 - \sin\theta_{eq})}{\cos\theta_{eq}^2} - K_2 \cos\theta_{eq}^2 - K_{1eff} \right] \quad (6)$$

Where $a = 1 + K_{1eff}/(2K_2)$, $b = \mu_0M_SH_{IP}/(4K_2)$, t_{FeCoB} and t_{MgO} are the storage layer and tunnel barrier thicknesses, μ_0 is the vacuum permeability and θ_{eq} is the magnetization angle in equilibrium.

The deterministic switching band is a result of the topology of the total energy density landscape of the system. At equilibrium and no applied voltage, we have that two stable states, P and AP, that are present and separated by an energy barrier. With the voltage modulation of the energy, the separation between P and AP becomes smaller until the voltage bias reaches a threshold value V_{IP} and there is no more distinction between these states, with \vec{m} relaxing into an in-plane state. If a voltage is applied with an amplitude larger than V_C and smaller than V_{IP} , but not high enough such that the damping will have time to dissipate energy preventing a double-crossing of the energy barrier, we achieve a switching regime that is uncorrelated to the pulse width past a critical pulse duration.

We can use a 3D representation of the energy landscape with the \vec{m} time-trace to see the dynamics of this regime in Fig.2. The magnetization is first allowed to relax before applying a 1ns voltage pulse at $\tau = \tau_{on}$ with 0.5V amplitude. We see \vec{m} follow the isolines of the landscape as the damping dissipates energy and it crosses hemispheres, representing a half-precession and a reversal. With the pulse still on, the leftover energy becomes smaller than the energy barrier at 0.5V, forcing \vec{m} to precess around the P stable state. When the pulse is turned off at $\tau = \tau_{off}$ it will relax to the original P equilibrium state at 0V in Fig.2b.

The range of voltage for which this happens cannot be calculated analytically, requiring numerical simulations to study it as it depends on energy dissipation. The two parameters that will influence it more strongly are the Gilbert damping and the total effective anisotropy. The first one dictates how fast the energy dissipation during the precession occurs, thereby defining the precession frequency. The second will change the energy of the system and the energy barriers that separate each state. With larger anisotropy, the voltage range for this

regime also increases. Additionally, there is a specific state that will be responsible, along with the damping, for the relaxation behavior of \vec{m} that results in the features of the phase diagram that are hidden at higher temperatures: the existence of a saddle point, which is very sensitive to thermal fluctuations. At finite temperatures, there is an immediate reduction of the switching probability. The switching band, for instance, loses its deterministic nature for temperatures above 50K with high reliability deterministic switching only expected for sub-10K operation.

This regime has potential applications in the context of low energy systems and cryoelectronics. As the write energy scales with V_C^2 , we explore experimentally the magnitude of VCMA, the coefficient ξ , and how it is possible to optimize it through stack engineering.

III. EXPERIMENTAL RESULTS

Perpendicular anisotropy magnetic tunnel junctions were fabricated on 100mm wafers to study the influence of the FeCoB storage layer and MgO tunnel barrier thicknesses on ξ . The devices are made with an out-of-plane magnetized FeCoB storage layer with the following structure for the MTJ: W(0.3)/FeCoB(0.9)/Mg(0.5-1.2)/Ox(15s)/Mg(0.5-1.2)/Ox(15s)/Mg(0.5)/FeCoB(0.8-1.6), where numbers are the layer thickness in nm. The Mg and FeCoB of the storage layer are deposited as a wedge, with their thickness varying within the indicated range across the wafer. The tunnel barrier consists of naturally oxidized double Mg wedge under 150mbar of O_2 pressure and Ox represents the oxidation time in seconds. Fig.3 shows the stack cross-wedge with a synthetic antiferromagnet (SAF) with the structure $[Co/Pt]_6/Ru/[Co/Pt]_3$. The wedges are fabricated 90deg in relation to each other, which gives us all possible combinations of thicknesses for both layers. In (c) the effects of a DC bias voltage on the field hysteresis loop of a random device is shown with a decrease of coercivity at negative bias, which is evidence of VCMA in our sample. The stray field of -350 Oe in the measurements is originated from a non-compensated SAF, which can be corrected by adjusting the number of Co/Pt repetitions and reference layer thickness [13].

To extract ξ from these devices, we apply the method described in [14]. A DC phase diagram is measured by applying a sweeping out-of-plane magnetic field under DC bias, giving us the switching field dependence on applied voltage. The range used is limited to 0.8V, lower than the writing breakdown voltage of our devices (1.6V) at pulse widths close to 1ns. Fig.4a shows the average field-resistance loops at different applied voltages and Fig.4b the phase diagram, with a trend of increased/decreased coercivity for positive/negative bias. In the absence of parasitic effects and Joule heating, we should retrieve a perfectly triangular shape, as is characteristic of a VCMA with limited STT due to the low current levels at high RA ($> 100\Omega \cdot \mu m^2$).

Then, by fitting the parallel-to-antiparallel (PAP) and the antiparallel-to-parallel (APP) transitions simultaneously with

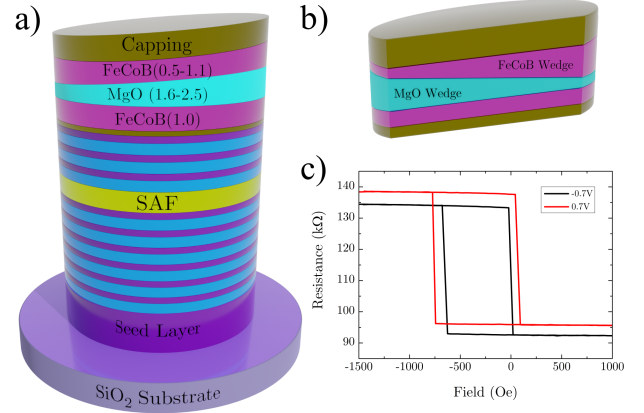


Fig. 3. a)Schematic representation of the full p-VCMA-MRAM. b)Cross section of the device's MTJ, showing the double wedge of FeCoB and MgO. c)Hysteresis loop of a device at 300K under 0.7V and -0.7V, with a reduction of coercivity for negative bias.

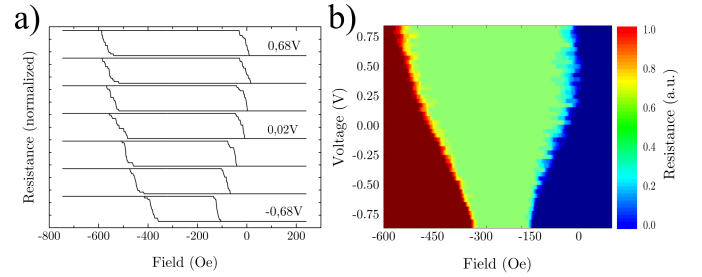


Fig. 4. a)Normalized field-resistance hysteresis loops for different applied voltages, from -0.68V to +0.68V. b)DC phase diagram at 300K showing the boundaries of the field switching for PAP and APP transitions, with normalized resistance.

the switching field equation, we can obtain the contributions from STT, VCMA and self heating from Eq.7 [14].

$$H_{sw}^{\pm} = \pm H_C + H_{RL} + \frac{\tau}{\alpha} \frac{V_b}{RA} \pm \epsilon V_b \mp \zeta \frac{V_b^2}{RA'} \quad (7)$$

Where H_{sw}^+ refers to the PAP and H_{sw}^- to the APP branch. H_C is the coercivity, H_{RL} is the stray field from the reference layer and $RA' = RA(1 + TMR|V_b|)(1 - 0.5|V_b|)$ is the voltage dependent resistance of the AP state. The STT factor τ/α is expected to have a smaller contribution. To further reduce this term, devices with RA of the order of $1k\Omega \cdot \mu m^2$ are necessary. The more relevant contribution will be from the VCMA term ϵ . It is equivalent to the coercivity modulation with voltage dH_C/dV_b , which gives us the linear slopes of the diagram in Fig.4b. They deviate from a perfectly triangular boundary mostly due to the Joule heating contribution ζ , that becomes increasingly prevalent at low temperatures as the MgO heat capacity decreases below 100K [15]. This effect can be seen in Fig.5, where the switching field boundaries for 280K, 80K and 10K are shown to become progressively more concave. As such, the joule heating at 10K induces a dominant polarity-independent effect on the observed coercivity.

Using the thermally assisted barrier-crossing model to estimate the anisotropy field from the extracted coercivity [16], we

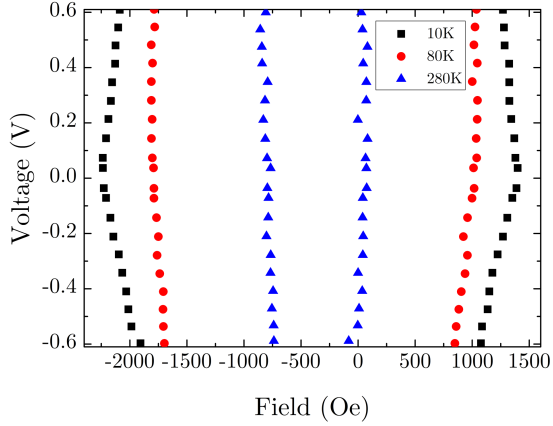


Fig. 5. Switching field boundaries for 280K, 80K and 10K in red, black and blue, respectively. The heating capacity reduction of MgO at low temperature is visible at 10K from the symmetrical effect V_b has on coercivity.

can calculate ξ using equations 7 and 8 [17], which requires the measurement 'a-priori' of the thermal stability Δ for each device that can be done by a separate measurement using a field switching probability distribution at zero bias (20mV) using the method described in [18].

$$\frac{\partial H_K}{\partial V_b} = \epsilon \left(1 - \frac{1}{2} \sqrt{\frac{\ln(\frac{\tau}{\tau_0})}{\Delta}} \right)^{-1} \quad (8)$$

$$\xi = \frac{M_S t_{FeCoB} t_{MgO}}{2} \frac{\partial H_K}{\partial V_b} \quad (9)$$

Where τ_0 is the attempt frequency $\approx 10^{-10}s$ and $\tau = 100ns$ is the measurement time. Taking into account a dead layer of 0.5nm in the FeCoB, extracted from MOKE analysis, and an $M_S = 1.3$ MA/m [19], ξ is calculated for a total of 1450 devices. Fig.6 shows a monotonic increase of ξ with effective FeCoB thickness at 300K with a maximum value of 22.9 fJ/Vm at 1.1nm. The maximum TMR measured in these devices is 115%, corresponding to a thicker FeCoB layer with 1.1nm. Therefore, the dependence we see does not cover the full range of thicknesses for which PMA exists in this sample and it deviates from the expected trend [20] [21]. A broader analysis is needed to verify if the linear proportionality continues for thicker layers or if there is a shift in this dependence when the demagnetization energy decreases even further the effective perpendicular anisotropy, at the transition to an in-plane state. The MgO dependence suggests highest VCMA coefficient for 2.2nm thickness and the oxidation conditions used, also corresponding to devices with highest TMR. Subsequently we measured three devices at 10K, observing an increase of the VCMA coefficient similarly to what was already previously reported [22], as shown by arrows in Fig. 6. ξ was calculated assuming $M_S(0K) = 1.45$ MA/m, reaching a maximum of 34 fJ/Vm. The Callen-Callen law [23] is applied to account for the increase of M_S with decreasing temperature.

We then investigate the VCMA effect dependence on the device's magnetic properties. In Fig.7, the ξ dependence with

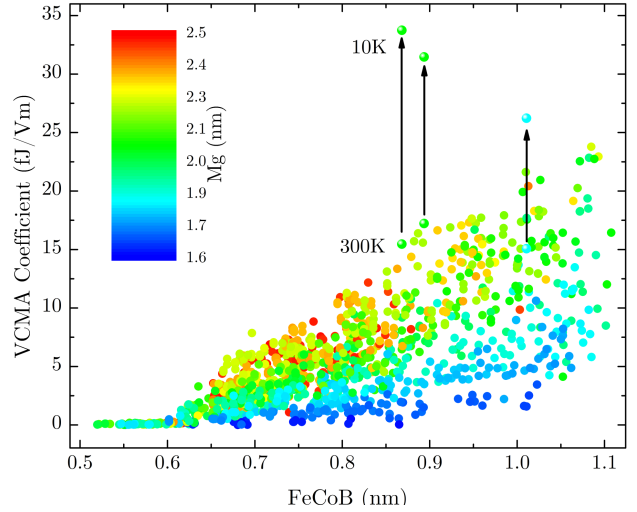


Fig. 6. Experimental variation of the VCMA coefficient ξ with effective FeCoB thickness of the storage layer and MgO tunnel barrier. The arrow represents the increase in VCMA measured on a single device at 5K.

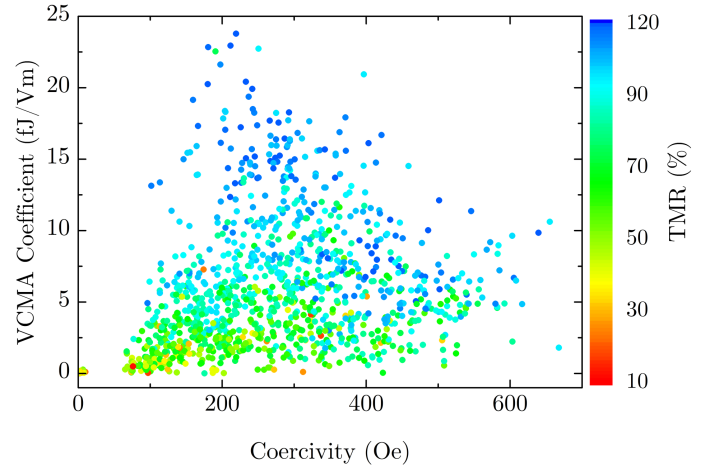


Fig. 7. Dependence of VCMA coefficient with device coercivity and tunneling magneto-resistance.

coercivity shows that it reaches a maximum at $\approx 250Oe$, not showing any clear proportionality. The TMR dependence, however, shows an increase in ξ for larger TMR values, suggesting that VCMA may also be dependent on the same factors influencing TMR and less dependent on the anisotropy of the storage layer, as ξ seems to be uncorrelated to coercivity. These statements are based on an expected proportionality between coercivity and the effective anisotropy of the storage layer, as well as TMR being an indicator of the FeCoB/MgO interface quality and tunnel barrier crystallinity. The modest values achieved for both TMR and VCMA also indicate that the MgO barrier used, with natural oxidation of the deposited metallic Mg and an Mg capping of 0.5nm induces large roughness levels on the interface with the storage layer, limiting the magnitude of both effects.

IV. CONCLUSION

By investigating the VCMA switching for low energy systems at temperatures below 50K, we predict the existence

of a deterministic switching regime that, coupled with lower switching energies, will be advantageous as a non-volatile memory technology, achieved by optimizing the material parameters of the MTJ. This was done using the described method on a wafer with thousands of devices that have each different thicknesses for the tunnel barrier and storage layers. It allows us to observe dependencies that are difficult to measure otherwise, such as the ξ dependence on both FeCoB and MgO thicknesses, meaning that the quality of the MTJ structure is crucial to achieve a high coefficient.

A more thorough analysis of device heating must be conducted to assess what is the real temperature at barrier-level with fast-pulse writing currents, rather than DC bias. Limiting the current by increasing the RA and optimizing ξ will reduce the impact of the Joule heating.

As the VCMA effect is enhanced at lower temperatures, implementing this memory in environments below 77K, or in deep cryogenics, can fill an existing gap where essential electronic components could be developed aiming at high-energy efficiency, which is also relevant in the context of quantum technologies and high performance computing.

ACKNOWLEDGMENT

This work was supported in part by the French National Research Agency under Project CRYMCO (ANR-20-CE24-0009) and in part by the European Research Council via grant MAGICAL ERC Adv 669204 and PEPR project PRESQUILE.

REFERENCES

- [1] N. Jones, "How to stop data centres from gobbling up the world's electricity," *Springer Nature Limited*, vol. 561, pp. 163–166, 2018. [Online]. Available: [www.https://www.nature.com/articles/d41586-018-06610-y](https://www.nature.com/articles/d41586-018-06610-y)
- [2] Y. Shiota, S. Miwa, T. Nozaki, F. Bonell, N. Mizuochi, T. Shinjo, H. Kubota, S. Yuasa, and Y. Suzuki, "Pulse voltage-induced dynamic magnetization switching in magnetic tunneling junctions with high resistance-area product," *Applied Physics Letters*, vol. 101, no. 10, p. 102406, 2012. [Online]. Available: <https://doi.org/10.1063/1.4751035>
- [3] W. G. Wang and C. L. Chien, "Voltage-induced switching in magnetic tunnel junctions with perpendicular magnetic anisotropy," *Journal of Physics D: Applied Physics*, vol. 46, no. 7, p. 074004, jan 2013. [Online]. Available: <https://dx.doi.org/10.1088/0022-3727/46/7/074004>
- [4] S. Kanai, Y. Nakatani, M. Yamanouchi, S. Ikeda, H. Sato, F. Matsukura, and H. Ohno, "Magnetization switching in a cofeb/mgo magnetic tunnel junction by combining spin-transfer torque and electric field-effect," *Applied Physics Letters*, vol. 104, no. 21, p. 212406, 2014. [Online]. Available: <https://doi.org/10.1063/1.4880720>
- [5] L. Rehm, G. Wolf, B. Kardasz, M. Pinarbasi, and A. D. Kent, "Sub-nanosecond spin-torque switching of perpendicular magnetic tunnel junction nanopillars at cryogenic temperatures," *Applied Physics Letters*, vol. 115, no. 18, p. 182404, 2019. [Online]. Available: <https://doi.org/10.1063/1.5128106>
- [6] C. Grezes, F. Ebrahimi, J. G. Alzate, X. Cai, J. A. Katine, J. Langer, B. Ocker, P. Khalili Amiri, and K. L. Wang, "Ultra-low switching energy and scaling in electric-field-controlled nanoscale magnetic tunnel junctions with high resistance-area product," *Applied Physics Letters*, vol. 108, no. 1, p. 012403, 2016. [Online]. Available: <https://doi.org/10.1063/1.4939446>
- [7] W. Kang, Y. Ran, Y. Zhang, W. Lv, and W. Zhao, "Modeling and exploration of the voltage-controlled magnetic anisotropy effect for the next-generation low-power and high-speed mram applications," *IEEE Transactions on Nanotechnology*, vol. 16, no. 3, pp. 387–395, 2017.
- [8] A. Okada, S. Kanai, S. Fukami, H. Sato, and H. Ohno, "Electric-field effect on the easy cone angle of the easy-cone state in cofeb/mgo investigated by ferromagnetic resonance," *Applied Physics Letters*, vol. 112, no. 17, p. 172402, 2018. [Online]. Available: <https://doi.org/10.1063/1.5026418>
- [9] S. E. Barnes, J. Ieda, and S. Maekawa, "Rashba spin-orbit anisotropy and the electric field control of magnetism," *Scientific Reports*, vol. 4, 2014. [Online]. Available: <https://doi.org/10.1038/srep04105>
- [10] J. Slonczewski, "Current-driven excitation of magnetic multilayers," *Journal of Magnetism and Magnetic Materials*, vol. 159, no. 1-2, pp. L1–L7, Jun. 1996. [Online]. Available: <https://linkinghub.elsevier.com/retrieve/pii/0304885396000625>
- [11] "Second order anisotropy contribution in perpendicular magnetic tunnel junctions," *Scientific Reports*, vol. 6, no. 1, pp. 2045–2322, 2016. [Online]. Available: <https://doi.org/10.1038/srep26877>
- [12] A. Hubert and R. Schäfer, "Magnetic domains: the analysis of magnetic microstructures," *Springer Science Business Media*, 2008.
- [13] P. B. Veiga, A. Mora-Hernandez, M. Dammak, S. Auffret, I. Joumard, L. Vila, L. D. Buda-Prejbeanu, I. L. Prejbeanu, B. Dieny, and R. C. Sousa, "Control of interface anisotropy for spin transfer torque in perpendicular magnetic tunnel junctions for cryogenic temperature operation," *AIP Advances*, vol. 13, no. 2, p. 025253, 2023. [Online]. Available: <https://doi.org/10.1063/9.0000512>
- [14] G. Mihajlovic, N. Smith, T. Santos, J. Li, M. Tran, M. Carey, B. Terris, and J. Katine, "Origin of the resistance-area-product dependence of spin-transfer-torque switching in perpendicular magnetic random-access memory cells," *Phys. Rev. Appl.*, vol. 13, p. 024004, Feb 2020. [Online]. Available: <https://link.aps.org/doi/10.1103/PhysRevApplied.13.024004>
- [15] T. H. K. Barron, W. T. Berg, J. A. Morrison, and E. W. R. Steacie, "On the heat capacity of crystalline magnesium oxide," *Proceedings of the Royal Society of London. Series A. Mathematical and Physical Sciences*, vol. 250, no. 1260, pp. 70–83, 1959. [Online]. Available: <https://royalsocietypublishing.org/doi/abs/10.1098/rspa.1959.0051>
- [16] M. P. Sharrock, "Time dependence of switching fields in magnetic recording media (invited)," *Journal of Applied Physics*, vol. 76, pp. 6413–6418, 1994.
- [17] Y. Wu, K. Garello, W. Kim, M. Gupta, M. Perumkunnil, V. Kateel, S. Couet, R. Carpenter, S. Rao, S. Van Beek, K. Vudya Sethu, F. Yasin, D. Crotti, and G. Kar, "Voltage-gate-assisted spin-orbit-torque magnetic random-access memory for high-density and low-power embedded applications," *Phys. Rev. Appl.*, vol. 15, p. 064015, Jun 2021. [Online]. Available: <https://link.aps.org/doi/10.1103/PhysRevApplied.15.064015>
- [18] L. Tillie, E. Nowak, R. Sousa, M.-C. Cyrille, B. Delaet, T. Magis, A. Persico, J. Langer, B. Ocker, I.-L. Prejbeanu, and L. Perniola, "Data retention extraction methodology for perpendicular STT-MRAM," in *Electron Devices Meeting (IEDM), 2016 IEEE International*, San Francisco, United States, Dec. 2016. [Online]. Available: <https://hal.science/hal-01718116>
- [19] L. Chuchet, "Magnetic and transport properties of single and double perpendicular magnetic tunnel junctions," Theses, Université Grenoble Alpes, Nov. 2015. [Online]. Available: <https://theses.hal.science/tel-01312194>
- [20] Y.-C. Lau, P. Sheng, S. Mitani, D. Chiba, and M. Hayashi, "Electric field modulation of the non-linear areal magnetic anisotropy energy," *Applied Physics Letters*, vol. 110, no. 2, p. 022405, 2017. [Online]. Available: <https://doi.org/10.1063/1.4973700>
- [21] J. Lourembam, J. Huang, S. T. Lim, and E. F. Gerard, "Role of cofeb thickness in electric field controlled sub-100 nm sized magnetic tunnel junctions," *AIP Advances*, vol. 8, no. 5, p. 055915, 2018. [Online]. Available: <https://doi.org/10.1063/1.5006368>
- [22] J. G. Alzate, P. Khalili Amiri, G. Yu, P. Upadhyaya, J. A. Katine, J. Langer, B. Ocker, I. N. Krivorotov, and K. L. Wang, "Temperature dependence of the voltage-controlled perpendicular anisotropy in nanoscale mgo/cofeb/ta magnetic tunnel junctions," *Applied Physics Letters*, vol. 104, no. 11, p. 112410, 2014. [Online]. Available: <https://doi.org/10.1063/1.4869152>
- [23] K.-M. Lee, J. W. Choi, J. Sok, and B.-C. Min, "Temperature dependence of the interfacial magnetic anisotropy in w/cofeb/mgo," *AIP Advances*, vol. 7, no. 6, p. 065107, 2017, Eq.1, coefficient used: 1.73. [Online]. Available: <https://doi.org/10.1063/1.4985720>